Investigation of the active sites and optimum Pd/Al of Pd/ZSM–5 passive NO adsorbers for the cold-start application: Evidence of isolated-Pd species obtained after a high-temperature thermal treatment

Jaeha Lee[a], YoungSeok Ryou[a], Sung June Cho[b], Hyokyoung Lee[c], Chang Hwan Kim[c], Do Heui Kim[a],*

[a] School of Chemical and Biological Engineering, Institute of Chemical Processes, Seoul National University, Seoul, 151-744 Republic of Korea
[b] Clean Energy Technology Laboratory and Department of Applied Chemical Engineering, Chonnam National University, Gwangju 500-757, Republic of Korea
[c] Hyundai-Kia Motors R&D center, Hwaseong, 445-706 Republic of Korea

ARTICLE INFO

ABSTRACT

We investigated the chemisorptive NO adsorption ability at a low temperature (120 °C) of the Pd/ZSM–5 passive NO_x adsorbers (PNA) to address the cold-start NO_x emission. The Pd/ZSM–5 showed a much higher NO adsorption ability after the oxidative treatment at 750 °C compared with the 500 °C treatment; according to the combined EXAFS, XPS and XRD results, atomically dispersed Pd species were formed over the former, while small PdO agglomerates were observed over the latter. The Pd species on the Pd/ZSM–5 were further examined by applying a NH_4NO_3-titration method, where an ion exchange occurred with only the ionic Pd in the zeolite. When the Pd(2)/ZSM–5 was treated at 750 °C, it exchanged ions with an NH_4NO_3 solution whereby most of the Pd was ion-exchanged, and this resulted in a decreased NO adsorption capability. Alternatively, a much lesser amount of ion-exchanged Pd was found on the Pd/ZSM–5 that was treated at 500 °C. The combined results indicate that the ionic-Pd species on the ZSM–5, not the bulk PdO, are the active sites for the chemisorptive NO adsorption at the low temperature. The NO adsorption capability was also investigated as a function of the Pd loading and the Si-to-Al_2 molar ratio of the ZSM–5. The results suggest that an optimum Pd-to-Al molar ratio exists for the Pd/ZSM–5 with the maximum NO adsorption capability, which was found at around 0.25, thereby suggesting that the Al in the ZSM–5 framework led to the high dispersion of the ionic-Pd species up to the optimum Pd/Al ratio. Above the optimum Pd/Al ratio, however, the bulk-PdO phase formed on the ZSM–5 resulting in a lower NO adsorption capability; that is, the ZSM–5 with the higher Al content required a higher Pd amount for the attainment of the optimum NO adsorption capability. In summary, the chemisorptive NO adsorption at the low temperature is significantly influenced by both the Si-to-Al_2 molar ratio and the Pd-to-Al molar ratio of the Pd/ZSM–5 catalysts.

1. Introduction

Reducing the nitrogen oxide (NO_x)-emission from lean-burn engines remains a great challenge of the automotive industry [1]. The NO_x-storage reduction (NSR) [2,3] and selective catalytic reduction (SCR) [4–10] technologies have been successfully implemented for the reduction of NO_x emissions; however, their usage in the low-temperature regime is limited. NSR requires temperatures as high as 250 °C for the NO-to-NO_2 oxidization that is followed by the storage of the NO_2 in alkaline-earth materials (e.g., barium oxide) or alkali metals (e.g., potassium oxide) in a nitrate form [3]. The SCR operating temperature is lower than that of the NSR, but the system still requires temperatures as

high as 200 °C to sufficiently convert NO_x into nitrogen gas (N_2) [5–7]. Even though the catalytic efficiency of the NSR and SCR are satisfactory once they reach their respective operating temperatures, neither can reduce the NO_x effectively below their operating-temperature ranges. Thus, during the cold-start period of an automobile when the temperatures are not sufficiently high, the NO_x species that are released into the atmosphere have not been converted by catalysts [11].

It has been reported that the majority of vehicular NO_x emissions occur during the cold-start period that is prior to the attainment of the minimum operating temperature by each of the SCR and NSR catalysts [11]. Since more stringent NO_x-emission regulations will be enforced in the near future [1], the cold-start NO_x-emission control presents a

major challenge [12]. The three-way conversion (TWC) catalysts for the gasoline engine can reach their operating temperature relatively quickly because they are typically placed close to the engine-out position, and the feed-gas temperatures are higher [12]. Alternatively, the diesel engine requires more than 100 s for the catalytic components to reach their operating temperatures because of a low exhaust temperature [12,13].

Recently, Chen et al. reported the application of palladium (Pd)/ zeolite catalysts in a diesel engine for the trapping of NO_x during the cold-start period and the release of the NO_x at elevated temperatures where the SCR and NSR catalysts can reduce the NO_x [14]. They not only showed the superior NO adsorption ability of the Pd/zeolite catalysts at low temperatures (80–120 °C), but they also showed a sound hydrothermal stability and a sulfur tolerance [14]. They proposed that the framework structure of the supporting zeolite plays a key role in the NO adsorption ability of Pd/zeolite catalysts, where the Pd that was supported on the smaller-pore zeolite interacted more strongly with the NO thereby releasing the NO_x at higher temperatures [14]. That is, Pd species are capable of the chemisorption of NO at low temperatures to reduce the NO_x emission during the cold-start period. Some NO species are known to catalytically transform into NO_2 or are reduced to N_2 by hydrocarbons during the entire process [14]. Recent patent publications by Jonson Matthey Company regarding the NO_x-trap catalysts during the cold-start period for the diesel engine also considered Pd/ zeolite as a strong candidate material for real-world applications [15–17]. Several recent publications also suggested that Pd/zeolite could be the candidate catalyst for cold-start applications [18,19].

In addition, from the mid-1990s to the early 2000s, the supporting of Pd on zeolite catalysts gained considerable attention as the candidate catalysts for the hydrocarbon SCR [20,21]. Especially, many works have been published regarding the CH_4–SCR activity over the Pd/ Zeolite Socony Mobile–5 (ZSM–5) catalysts [22–30]. Some consensus regarding the CH_4–SCR mechanism of the Pd/ZSM–5 has been made, where the NO that is adsorbed on the isolated Pd reacts with CH_4 for its conversion to N_2 [25,29]. Although the exact Pd state that can adsorb NO remains as a matter of debate [27,31], Ogura et al. proved that the cationic species of the palladium(II) ion, Pd^{2+}, should be the active sites for the CH_4–SCR reaction based on the sodium chloride (NaCl)-titration method [27]. However, Pd/ZSM–5 showed only a slight CH_4–SCR activity below 300 °C [23,28], and the utilization of the NO adsorption ability of Pd/ZSM–5 for the trapping of NO that is emitted below 200 °C has gained only a minor attention until recently. To utilize the Pd/ZSM–5 as a catalyst for the reduction of the NO_x emission during the cold-start period, the Pd/ZSM–5 chemisorptive properties should be investigated extensively.

Murata et al. recently reported that Pd/ZSM–5 can trap NO at low temperatures [32]. They attempted to optimize the catalyst by varying the Pd loading and the silicon (Si)-to-aluminum (Al) ratio of the ZSM–5. This report, however, is considered as preliminary, since the main focus is the NO adsorption functionality of the Pd/ZSM–5 [32]. They did not characterize the interaction between Pd and the ZSM–5 in detail or explain the way that such an interaction would affect the NO adsorption ability of the Pd/ZSM–5. Moreover, the focus of their interest is the gasoline engine, not the lean-burn engine, since they used only a 2-vol % oxygen gas (O_2) in the reactant [32].

The focus of the present work is the chemisorption and desorption of NO on the Pd/ZSM–5 under lean conditions at low temperatures. The interaction between the Pd and the ZSM–5 with different Pd loadings and a differing Si-to-Al_2 molar ratio (SAR) were extensively investigated and characterized using X-ray diffraction (XRD), Raman spectroscopy, the X-ray absorption fine structure (XAFS) analysis, X-ray photon spectroscopy (XPS), the H_2 temperature-programmed reduction (H_2-TPR), the ammonia temperature-programmed reduction (NH_3-TPD), Al-alloy nuclear magnetic resonance (Al[Si]-NMR) and inductively coupled plasma atomic emission spectroscopy (ICP-AES). This interaction emerged as a critical factor not only in the determination of the Pd thermal stability but also in the determination of the NO adsorption ability of the Pd/ZSM–5 at a low temperature. In addition, the NO adsorption active sites on the Pd/ZSM–5 were also confirmed through the application of the modified titration method.

2. Experimental

2.1. Catalyst preparation

Ammonium (NH_4)-ZSM–5 with SARs of 23, 30, 50, 80 and ∼300 (Alfa Chemicals, U.K.) was ion-exchanged with palladium(II) nitrate hydrate, $Pd(NO_3)_2(H_2O)_2$ (Sigma-Aldrich, U.S.A.). More specifically, the desired amount of the $Pd(NO_3)_2(H_2O)_2$ was dissolved in 50 mL of deionized water (DIW), and 2 g of the ZSM–5 was added to the solution. The mixed solution was magnetically stirred at 600 rpm for 30 min at room temperature and transferred to a water bath that was maintained at 65 °C. The mixed solution was further magnetically stirred at 500 rpm for 20 h. The ion-exchanged ZSM–5 was filtered, washed with 1 L of the DIW, and then dried at 100 °C in an oven for 6 h. The nominal wt% of the dissolved Pd is denoted in the parenthesis of the sample name; for example, if $Pd(NO_3)_2(H_2O)_2$ corresponding to 2-wt% Pd was dissolved in water and ion-exchanged into the ZSM–5, it is denoted as

Table 1

Pd-content (wt%), Pd-to-Al molar-ratio and NO adsorption/desorption results of Pd/ZSM–5 catalysts. The optimum Pd loadings for the maximum NO adsorption on the ZSM–5 with the Si/Al$_2$ ratios of 23, 30 and 50 are marked with the bold text.

Catalyst	Pd content[a] (wt%)	Pd/Al[1]	NO_x desorbed[b] (μmol/$g_{catal.}$) (750C catalysts)		
			Below 300 °C	Above 300 °C	Total Amount
Pd(1)/ZSM-5 (Si/Al$_2$ = 23)	1.10	0.08	2.9	2.3	5.2
Pd(2)/ZSM-5 (Si/Al$_2$ = 23)	2.02	0.16	9.4	6.3	15.7
Pd(3)/ZSM-5 (Si/Al$_2$ = 23)	**2.71**	**0.26**	**9.1**	**8.0**	**17.1**
Pd(4)/ZSM-5 (Si/Al$_2$ = 23)	3.73	0.36	7.1	4.9	12.0
Pd(0.5)/ZSM-5 (Si/Al$_2$ = 30)	0.51	0.06	0.3	4.9	5.2
Pd(1)/ZSM-5 (Si/Al$_2$ = 30)	0.91	0.11	3.7	11.7	15.4
Pd(2)/ZSM-5 (Si/Al$_2$ = 30)	**1.90**	**0.24**	**8.9**	**15.7**	**24.6**
Pd(3)/ZSM-5 (Si/Al$_2$ = 30)	2.97	0.38	6.6	6.3	12.9
Pd(6)/ZSM-5 (Si/Al$_2$ = 30)	5.46	0.75	0.6	5.4	6.0
Pd(0.5)/ZSM-5 (Si/Al$_2$ = 50)	0.54	0.12	0	4.9	4.9
Pd(1)/ZSM-5 (Si/Al$_2$ = 50)	**1.02**	**0.23**	**0**	**8.3**	**8.3**
Pd(2)/ZSM-5 (Si/Al$_2$ = 50)	1.88	0.41	0	4.6	4.6
Pd(2)/ZSM-5 (Si/Al$_2$ = 80)	1.98	0.61	0	2.3	2.3
Pd(2)/ZSM-5 (Si/Al$_2$ = ∼300)	1.02	0.98	0	2.9	2.9

[a] From ICP-AES.

[b] From NO_x-TPD.

"Pd(2)/ZSM–5." The actual Pd loading and the resultant Pd-to-Al molar ratios of the prepared catalysts are listed in Table 1 based on the ICP-AES analysis. Except for the ZSM–5 with an SAR of ~300, most of the dissolved Pd was successfully ion-exchanged. The SAR of the ZSM–5 is denoted in the parenthesis after the sample name; for example, if 2-wt% Pd was loaded on the ZSM–5 with an SAR of 30, then it is named "Pd(2)/ZSM-5 (30)." All of the prepared catalysts were oxidized at 500 or 750 °C for 2 h during a 100 mL/min flow of 15-% O_2/N_2, and the respective designation of "500C" or "750C" was applied after the sample name (this temperature is sufficiently high to decompose the nitrate in the Pd precursor as determined by the ICP-AES analysis); for example, the Pd(2)/ZSM-5 that was oxidized at 750 °C was designated as "Pd(2)/ZSM-5 750C." All of the catalysts were characterized within 48 h of the preparation.

2.2. Catalyst evaluation

The NO adsorption/desorption tests were carried out in a continuous-flow quartz reactor, wherein 0.035 g of the catalyst was blended with 0.1 g of the alpha-phase Al oxide (α-Al_2O_3), where the volume ratio is 1:1. The temperature of the catalyst bed was measured by a type-K thermocouple that was inserted into the reactor and placed right above the catalyst bed. Prior to every NO adsorption/desorption test, the sample was pretreated with water (5%) and oxygen gas (10%), balanced with N_2 at a flow rate of 200 mL/min (GHSV of 120,000 h^{-1}) at 500 °C for 30 min, and then cooled to 120 °C in the same feed. The NO adsorption was performed by introducing 100 ppm of NO to the lean-gas mixture (10-% oxygen gas [O_2], 5-% water [H_2O] and an N_2 balance) for 100 s at 120 °C. When the NO was turned off and the NO concentration dropped below 1 ppm, the temperature was raised to 500 °C at the ramping rate of 10 °C/min, where it was maintained at 500 °C for 30 min during the flow of the lean-gas mixture for the full removal of the stored-NO_x species on the catalysts. Each NO adsorption/desorption test was repeated at least three times to check the reproducibility. In addition, to test the effect of carbon dioxide (CO_2) on the NO adsorption ability of the catalysts, 5% of CO_2 was added to the feed since CO_2 always exists in real-world engine exhausts. The NO was introduced into the reactor after the pretreatment step at 500 °C with the feed containing the CO_2. The effect of the CO_2 over the catalyst of the Pd(2)/ZSM–5 750C with a SAR of 30 is presented in Fig. S1, and this emerged as the best-performing catalyst in the evaluation of the present work. It was observed that the CO_2 provided only a minimal effect on the NO adsorption ability below 300 °C; therefore, the CO_2 was not added to the feed gas in the present study.

The NO_x concentration was measured using the 42i-HL NO_x analyzer (Thermo Fisher Scientific, U.S.A.). Fig. S2 shows the NO_x concentrations on the Pd(2)/ZSM–5 (30) 750C catalyst that was measured during the NO adsorption/desorption test as well as the NO concentration that was measured with the empty reactor. Upon the integration of the NO_x release profiles during the NO adsorption/desorption tests on the Pd(2)/ZSM-5 (30) 750C catalyst, the estimated released NO_x amount is comparable to the total NO amount that was introduced into the reactor. A slight discrepancy was observed, and this is probably because the NO_x analyzer cannot detect nitrogen species besides NO and NO_2 (e.g., N_2O). Since the error is small (less than 5%) in the present study, the adsorbed-NO amount on the catalyst can be estimated from the desorbed-NO_x amount during the temperature increase.

2.3. Characterization methods

The XRD patterns were taken using the Mode 1 Smartlab diffractometer (Rigaku, Japan) with Cu-Kα radiation (λ = 0.1542 nm) at a voltage and a current of 40 kV and 50 mA, respectively. The patterns were collected in a 2θ range from 5 to 90° with a scanning-step size of 0.02° at a speed of 2.5°/min. In the case of the fine XRD scan for the

observation of the small Pd oxide (PdO) peaks, the XRD scan rate was decreased to 0.2°/min.

The XPS analysis was performed using the K-alpha device (Thermo Fisher Scientific, U.K.) with an Al monochromatic (hν = 1486.6 eV) source. The charging effects were corrected with reference to the Si-2p binding energy of 103.3 eV. The spectra were processed using the CasaXPS software package (Casa Software, Japan). The surface composition of the catalysts was calculated using the integral intensities of the peaks that were normalized to the atomic-sensitivity factors that are reported in the reference [33].

The XAFS data of the catalyst over the Pd K-edge, which is 24350 eV under the ambient condition, was collected using the 7D-XAFS beamline of the Pohang Light Source (PLS-II) at the Pohang Accelerator Laboratory (South Korea), for which an Si(111) crystal was used as the monochromator, and the beam energy and the ring current are 2.5 GeV and 300 mA, respectively. An energy calibration of the Pd-foil samples was carried out (E_0 = 24,350 eV). The X-ray intensity for the signal of the Pd K-edge was monitored using ionization chambers that had been purged with pure N_2 at room temperature for the measurement of the incident (I_0) and fluorescent (I_f) beams. Bulk PdO was used as the reference compound. The respective step and duration times of the X-ray absorption near-edge spectroscopy (XANES) are 1.0 eV and 2 s, while for the EXAFS, they are 0.30 nm^{-1} and 3 s. The total number of points per XAFS spectrum is 478, and this is sufficient for the EXAFS analysis. In accordance with the literature, the obtained EXAFS data were analyzed using the Athena and Artemis computer programs (Demeter, U.S.A.) [34].

For the XAFS analysis, Artemis was implemented in the Demeter-program package (0.9.25) that was then utilized again after the data processing using Athena. The background removal was performed to extract the XAFS signal using the AUTOBK program (The University of Chicago, U.S.A.) for R_{bkg} = 0.1 nm, and the corresponding XAFS data in the k space were subsequently Fourier transformed with the Kaiser-Bessel window function, 10 nm^{-1} after the k^3 weighting, to amplify the high k information. The range for the Fourier transformation of the Pd samples Δk is from 30 to 130 nm^{-1}. The phase shifts and the amplitude functions of the reference were generated using FEFF6L (The University of Chicago, U.S.A.). The curve-fitting range in the r space Δr varied depending on the sample. The number of independent data points for the curve fit N_{idp} is determined using the Nyquist theory; as this number is always larger than the number of variables, the sufficient degree of freedom N_{var} is provided. The scattering path of the possible model structure was obtained from the FEFF6L calculation. Only the scatterings with a large contribution were included in the multishell fitting. The many-body reduction factor S_0^2 for the Pd of 0.9 was obtained from the curve fit of the XAFS data of the Pd foil under the same condition, and it was utilized further in the sample curve fit. The statistical quality of the curve fit or the proposed model can be determined from the R-factor that is available in the refinement.

The Raman-spectroscopy measurements were performed using the T64000 Raman spectrometer (Horiba Jobin Yvon, Japan) at the National Center for Inter-University Research Facilities (South Korea), for which an argon (Ar)-ion laser of a wavelength of 514.5 nm was used as a source.

The ICP-AES analysis, carried out using the Optima-4300 DV spectrometer (PerkinElmer, U.S.A.), measured the amount of ion-exchanged Pd in the ZSM–5 and the Pd-to-Al molar ratio of the prepared catalysts. For the analysis, 40 mg of the sample was dissolved in an aqua regia composed of 1.25 mL of concentrated nitric acid and 3.75 mL of concentrated hydrochloric acid.

A cryo-H_2-temperature programmed reduction (cryo-H_2-TPR) was performed using the BEL-CAT-II instrument (BEL Japan Inc., Japan) with a thermal conductivity detector (TCD). Prior to the measurement, 0.05 g of the sample was oxidized in a flow of 21-% O_2/N_2 at 750 °C for 2 h. After the pretreatment, the sample was cooled down to −90 °C and exposed to 5-% H_2/Ar. The temperature was raised from −90 to 900 °C

at a rate of 10 °C/min.

A temperature-programmed hydride decomposition (TPHD) was carried out using the BEL-CAT-II (BEL Japan Inc., Japan) again with a TCD, where 0.05 g of the sample was oxidized in a flow of 21-% O_2/N_2 at 750 °C for 2 h. Afterward, the catalysts were exposed to 5-% carbon monoxide (CO)/helium (He) for 30 min at 300 °C, and this was followed by a He purging at 400 °C for 1 h to remove the CO species from the catalysts. The temperature was cooled down to −90 °C, and the samples were exposed to the 5-% H_2/Ar. The temperature was then raised from −90 to 900 °C at a rate of 10 °C/min.

An ammonia temperature-programmed desorption (NH_3-TPD) profile was obtained using the BEL-CAT Basic instrument (BEL Japan Inc., Japan). Approximately 0.05 g of the prepared catalyst was loaded onto a quartz wool bed in a quartz U-shaped reactor. The sample was oxidized in a flow of 21-% O_2/N_2 at 750 °C for 2 h and then cooled to room temperature. Then, the sample was exposed to 5-% NH_3 balanced with He for 1 h, and this was followed by a pretreatment at 100 °C for 1 h to remove the weakly adsorbed NH_3 molecules from the surface. After the pretreatment, the samples were heated to 600 °C at the rate of 10 °C/min under a He flow.

^{27}Al and ^{29}Si magic-angle spinning (MAS) nuclear magnetic resonance (NMR) experiments were carried out on a WB Avance II 500 MHz (Bruker, Germany) system that was operated with a 4-mm MAS probe. A spinning frequency of 10 kHz, a spectral window of 65 kHz, complex points of 6572 and a pulse delay of 0.1 s were utilized to acquire 512 time-averaged scans.

N_2 adsorption/desorption isotherms were measured using the ASAP 2010 (Micromeritics Instruments, U.S.A.) apparatus at a liquid-N_2 temperature of −196 °C. Before the analysis, all of the catalysts were pretreated at 300 °C for 12 h under the evacuation condition. The mesopore volume and the specific surface area were calculated using the Barrett–Joyner–Halenda (BJH) and Brunauer–Emmett–Teller (BET) methods, respectively. The total-pore volume with a pore diameter of less than ∼70 nm was estimated using the single point adsorption at $P/P_0 = 0.97$. The micropore volume was calculated using the difference between the total-pore volume and the mesopore volume. The results are listed in Table S1.

2.4. NH₄NO₃ titration

The titration of the ionic Pd species followed the experimental procedure that was presented by Ogura et al. [27] with the exception of the use of an ammonium nitrate (NH_4NO_3) solution instead of an NaCl solution. Since residual Na ions could poison the NO adsorption capability of the catalysts, NH_4NO_3 was used because it can be easily removed by an oxidative treatment at an elevated temperature. A 1-M NH_4NO_3 solution was used for the NH_4NO_3 titration, and 0.5 g of the catalyst was stirred in 50 mL of the NH_4NO_3 solution for 20 h at 65 °C. After the filtration, the amount of Pd that was left in the catalyst was determined using ICP-AES. After the titration, each catalyst was reoxidized at 750 °C for 2 h allowing for the evaluation of the catalytic NO adsorption capability.

3. Result

3.1. Elucidation of the NO adsorption sites on the Pd/ZSM–5

Fig. 1 shows the NO_x desorption curves of the Pd(2)/ZSM–5 (30) after the oxidative treatments at 500, 600, 700, 750, 800 and 850 °C. The NO adsorption test was performed in a sequential order; for example, after the NO adsorption test was performed on the Pd(2)/ZSM-5 (30) 500C, the catalyst was oxidized at 600 °C for 2 h and another NO adsorption test was performed. The amount of NO_x that was adsorbed on the sample is tabulated in Table 2. As observed in Fig. 1 and Table 2, the amount of NO that had adsorbed on the Pd(2)/ZSM–5 was drastically increased from 10.6 to 24.6 μmol/g_{catal} when the oxidation
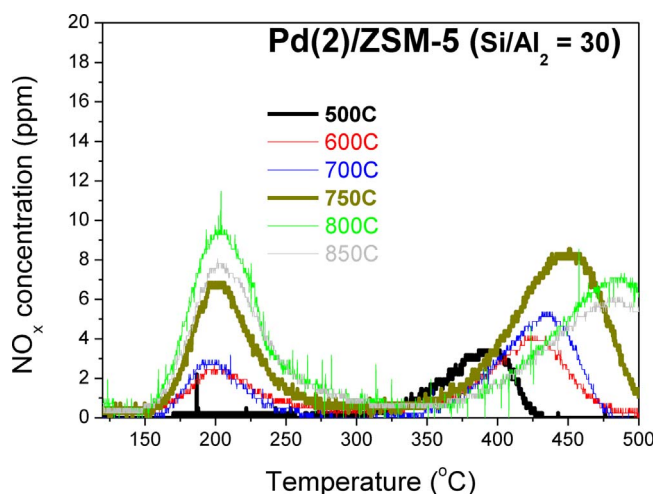

Fig. 1. NO_x desorption curve of the Pd(2)/ZSM–5 (Si/Al$_2$ = 30) catalyst after the oxidative treatments at various temperatures for 2 h.

Table 2
NO adsorption/desorption results of Pd/ZSM–5 catalysts after oxidative treatments at different temperatures from 500 to 850 °C. The NO adsorption ability was drastically increased after the oxidative treatment at 750 °C.

Pd(2)/ZSM–5 (Si/Al$_2$ = 30)	Low T (μmol/g_{catal}.)	High T (μmol/g_{catal}.)	Total (μmol/g_{catal}.)
500C	0.3	4.3	4.6
600C	3.7	6.9	10.6
700C	2.9	7.7	10.6
750C	8.9	15.7	24.6
800C	13.7	12.6	26.3
850C	11.7	11.4	23.1

temperature was increased from 700 to 750 °C. Two NO_x desorption peaks that were centered at ∼200 and ∼450 °C were simultaneously enhanced when the oxidation temperature was raised from 700 to 750 °C. The amount of NO that was adsorbed on the Pd(2)/ZSM–5 (30) reached the maximum value of 26.3 μmol/g_{catal} after an oxidative treatment at 800 °C, and this was diminished to 23.1 μmol/g_{catal} after an oxidative treatment at 850 °C; however, this variation is relatively small compared with the enhanced NO adsorption ability of the Pd(2)/ZSM–5 (30) after the oxidation at 750 °C. At the oxidation temperatures above 800 °C, the NO_x desorption peak at ∼450 °C shifted to the higher temperature of ∼490 °C, while a slight change of the NO_x desorption peak was observed at ∼200 °C. It should be emphasized that the Pd/ZSM–5 (30) that was treated above 800 °C shows a shift of the NO_x desorption peak toward higher temperatures, which is undesirable for the typical operation of a diesel vehicle (< 500 °C). Thus, it can be summarized that the Pd/ZSM–5 (30) 750C demonstrated the most desirable NO adsorption/desorption properties. Therefore, the Pd(2)/ZSM–5 (30) 500C and 750C samples were chosen for an investigation of the detailed physicochemical changes in the Pd species that were observed after the thermal treatment at 750 °C.

Fig. 2 shows the NO_x desorption profile of the catalyst of the Pd(2)/ZSM–5 (30) 750C, where the NO- and NO_2 desorption curves are plotted separately. The NO_x desorption peak below 300 °C consists of an almost-1:1 ratio of NO and NO_2, while the NO_x desorption peak above 300 °C mainly consists of NO. This finding implies that the NO adsorption on the Pd/ZSM–5 at low temperatures is not a simple adsorption process but is instead a chemisorption process that is accompanied by a transformation of NO into NO_2. Therefore, high temperatures are required to desorb chemisorbed NO. The details of the NO adsorption sites for the Pd/ZSM–5 are further examined in the "Discussion" section.
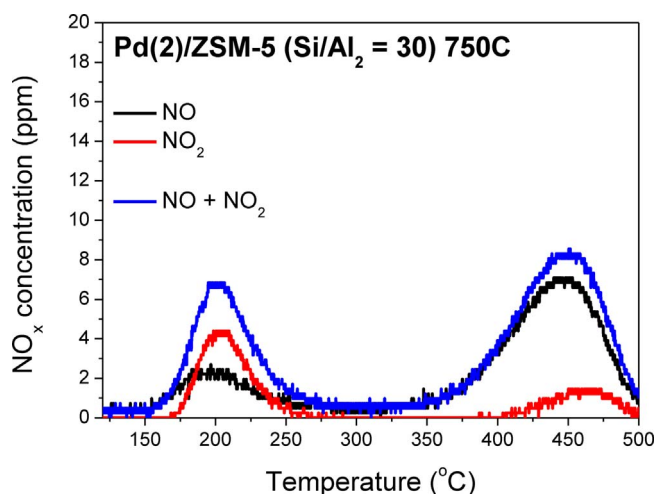
Fig. 2. NO_x desorption curve of the Pd(2)/ZSM–5 (Si/Al$_2$ = 30) 750C catalyst, which is among the most active catalysts that were investigated in the present work. The NO desorption curve and the NO_2 desorption curve are plotted separately.
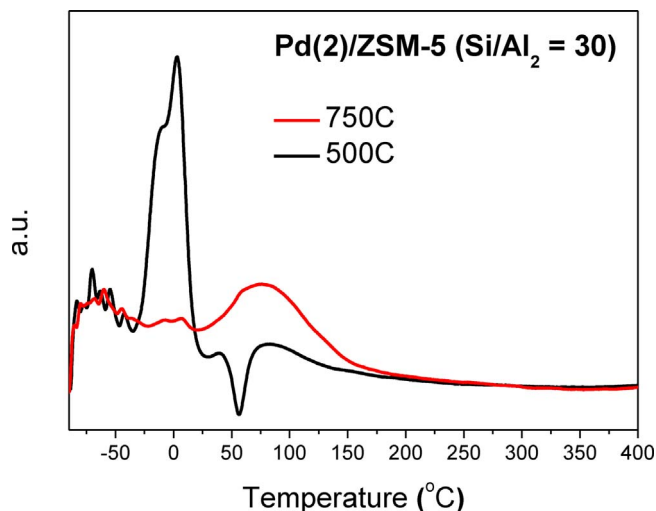

Fig. 3. Cryo-H_2-TPR curves of the Pd(2)/ZSM–5 (Si/Al$_2$ = 30) 500C and 750C catalysts.

Fig. 3 shows the H_2-TPR curves of the Pd(2)/ZSM–5 (30) after the oxidative treatments at 500 and 750 °C. The peaks below −20 °C in the H_2-TPR profiles are artifacts that originate from the desorption of the Ar gas that was adsorbed in the zeolite [35]. The Pd(2)/ZSM–5 (30) 500C demonstrated a huge reduction peak at ~0 °C and a negative peak at ~60 °C, which could be attributed to the reduction of the bulk PdO to Pd and the formation of the Pd hydride, and the decomposition of palladium hydride (PdH_x), respectively [35]. Alternatively, only a broad reduction peak ranging from ~50 to 150 °C was observed on the Pd(2)/ZSM–5 (30) 750C, which could be due to the reduction of the ionic-Pd species [35]. It is clearly evident in Fig. 3 that, when the oxidation temperature was increased from 500 to 750 °C, the reduction peak that originated from the bulk PdO disappeared, whereas that from the ionic-Pd species appeared; that is, the oxidative treatment at 750 °C redistributed the bulk-PdO species on the ZSM–5 (30). Since, according to Fig. 1, the treatment at 750 °C activated the NO adsorption ability of the Pd/ZSM–5 (30), it could be claimed that the redistribution of the bulk PdO and the formation of the ionic-Pd species are closely related to the NO adsorption ability of the Pd(2)/ZSM-5 (30).

Fig. 4 shows the EXAFS spectra of the catalysts of the Pd(2)/ZSM-5 (30) 500C and 750C. The Fourier transforms of the k^3-weighted EXAFS oscillation from the k space to the R space were performed over the range of 30–120 nm^{-1} to obtain the radial distribution function. The

bulk-PdO spectrum in Fig. 4 serves as a reference. In the Fourier transform of the bulk PdO, the two peaks that appear at 0.16 and 0.29 nm originate from the Pd–O and the Pd–Pd of the Pd–O–Pd bonds, respectively. In the spectrum of the Pd(2)/ZSM-5 (30) 500C, an intense Pd–O–Pd peak was observed, indicating the presence of the bulk PdO. In the Fourier-transformed spectrum of the Pd(2)/ZSM-5 (30) 750C, however, only the Pd–O peak at 0.16 nm was observed. Table 3 presents the curve-fitting analysis results for the EXAFS spectra of the Pd(2)/ZSM-5 (30) 500C and 750C. It is evident that the coordination number of the Pd second shell (Pd–O–Pd) was decreased from 3.0 ± 3.0 to 0 after the oxidative treatment at 750 °C indicating that the small PdO clusters on the Pd(2)/ZSM–5 were redispersed. Okumura et al. also reported that when Pd was ion-exchanged into the ZSM–5 with a high Al content, the Pd second shell was not observed on the R space of the EXAFS spectra, because the Al sites of the ZSM–5 stabilized the atomically dispersed Pd species [30].

The redispersion of the PdO was also confirmed on the XRD patterns of the Pd(2)/ZSM–5 that were taken after the oxidative treatments at 500 and 750 °C as shown in Fig. S3. To improve the resolution of the XRD pattern, the X-ray duration time was changed from 2.5 to 0.2°/min. The XRD peak from the PdO phases at 33.5 and 33.9° on the Pd(2)/ZSM-5 500C disappeared after the oxidation at 750 °C, and this is in agreement with the EXAFS results. The redispersion of an impregnated metal on zeolite after a high-temperature treatment has been also reported by Wang et al., who observed that copper monoxide (CuO) species that had precipitated on the external surface of the SAPO-34 migrated to the ion-exchange sites after a hydrothermal treatment at 700 °C [36]. A similar phenomenon is expected to occur on the Pd/ZSM–5 catalysts during the thermal treatment at 750 °C. Fig. S4 shows the XPS spectra of the Pd(2)/ZSM–5 catalysts after the oxidative treatments at 500 and 750 °C. The Pd species on the surface of the ZSM–5 exist in the 2+ state, since the Pd-3d$_{5/2}$ peak appeared at the binding energy of approximately 337 eV. In addition, the XANES spectra also show that the Pd species on the ZSM–5 (30) are in the +2 oxidative state (data not shown). Fig. S4 shows that after the oxidative treatment at 750 °C, the amount of Pd species on the surface, as calculated by XPS, was decreased substantially. Compared with the catalyst of the Pd(2)/ZSM-5 (30) 500C, the Pd-to-Si molar ratio on the catalyst of the Pd(2)/ZSM-5 (30) 750C was decreased from 0.032 to 0.006. This observation strongly suggests that the Pd species migrated into the ion-exchange sites during the oxidative treatment at 750 °C leading to a low Pd/Si amount on the surface as obtained by the XPS. Wang et al. also reported that the Cu-to-Si molar ratio, as measured by XPS, was decreased after the 700-°C hydrothermal treatment because the CuO species on the surface of the SAPO-34 migrated into the ion-exchange sites [36]. Ogura et al. also reported that the highly dispersed Pd in the ZSM–5 was not detected by the XPS unlike the Pd species on silicon dioxide (SiO_2) [27].

The combined H_2-TPR (Fig. 3), EXAFS (Fig. 4), XRD (Fig. S3) and XPS results (Fig. S4) strongly suggest that well-dispersed Pd species are generated after an oxidative treatment at 750 °C. Therefore, it seems that the well-dispersed Pd species on the ZSM–5 are NO adsorption sites leading to the activation of a NO adsorption capability after an oxidation at 750 °C. The bulk-like PdO species on the Pd/ZSM–5 catalyst seem to be inactive in the adsorption of NO. To confirm this hypothesis, the NH_4NO_3 titration was performed. A verification of the ability of the NH_4^+ ion to perform an exchange with the ionic-Pd species in zeolite is expected, and this results in the removal of the ionic Pd, while the bulk-PdO species remain in the ZSM–5. This was previously verified by Ogura et al., who reported that only the ionic-Pd species on the ZSM–5, not the bulk-PdO species, could be ion-exchanged with an NaCl solution [27]. When the Pd(2)/ZSM-5 (30) 750C was ion-exchanged with NH_4NO_3, the Pd concentration was decreased substantially from 1.9 to 0.4 wt% as shown by the ICP-AES results in Table 4; that is, 79% of the Pd species was removed from the catalyst. Alternatively, when the catalysts of the Pd(2)/ZSM-5 (30) 500C and Pd(2)/ZSM-5 (300) 750C
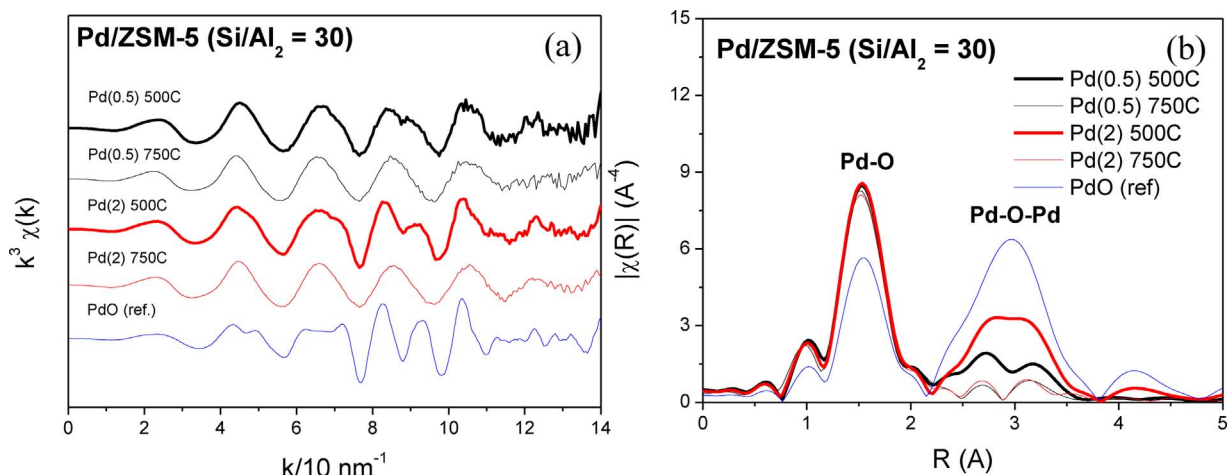
Fig. 4. (a) k^3-weighted Pd K-edge EXAFS oscillations and (b) their corresponding Fourier transforms for the bulk-PdO and Pd/ZSM–5 (Si/Al$_2$ = 30) catalysts.

Table 3
Summary of the curve-fitting of the Pd K-edge EXAFS data for the Pd(2)/ZSM–5 (30) 500C and 750C catalysts.

Pair	CN	Distance (nm)	DW factor (pm^2)	DE (eV)	R-factor
Pd(2)/ZSM–5 (Si/Al$_2$ = 30) 500C					
Pd–O	3.2 ± 0.4	0.201 ± 0.001	7 ± 13	12.7 ± 1.6	0.02
Pd–Pd	3.0 ± 3.0	0.308 ± 0.002	75 ± 77		
Pd–O	–	0.372 ± 0.002	–		
Pd(2)/ZSM–5 (Si/Al$_2$ = 30) 750C					
Pd–O	3.3 ± 0.2	0.201 ± 0.001	12 ± 17	11.0 ± 0.0	0.004
Pd–Pd	–	0.300 ± 0.004	–		
Pd–O	–	–	–		

Table 4
Residual amounts of Pd and Al on the Pd/ZSM–5 after an ion exchange with NH$_4$NO$_3$.

Catalyst	Pd (wt%)[a]	Al (wt%)[a]
Pd(2)/ZSM–5 (Si/Al$_2$ = 30)	1.90	2.10
750C → NH$_4$NO$_3$ ION	0.40	2.10
500C → NH$_4$NO$_3$ ION	1.07	2.10
Pd(2)/ZSM–5 (Si/Al$_2$ = ~300)	1.04	0.26
750C → NH$_4$NO$_3$ ION	0.77	0.26

[a] From ICP-AES.

Fig. 5. NO$_x$ desorption curves of the Pd(2)/ZSM–5 (Si/Al$_2$ = 30) catalyst after the extraction of the ionic-Pd species with NH$_4$NO$_3$ and a further oxidizing of the catalyst at 750 °C for 2 h.

were ion-exchanged with NH$_4$NO$_3$, both of which showed a minor NO adsorption ability, a smaller amount of Pd was removed from the catalysts. In the case of the Pd(2)/ZSM-5 (30) 500C, a 1.07-wt% Pd (out of 1.90 wt%) remained in the catalyst and in the case of the Pd(2)/ZSM-5 (300) 750C, a 0.77-wt% Pd (out of 1.04 wt%) remained in the catalyst. Therefore, as presented in Table 4, only 44 and 26% of the Pd species were removed from the Pd(2)/ZSM-5 (30) 500C and Pd(2)/ZSM-5 (300) 750C, respectively. Since the higher Pd amount was removed from the catalyst with the higher NO adsorption ability, it could be claimed that the Pd^{2+} species in the ZSM–5 are the NO adsorption sites. Similar to the present approach, Ogura et al. ion-exchanged Pd-loaded ZSM–5 catalysts with an NaCl solution and found that the catalytic activity of the NO$_2$–CH$_4$–O$_2$ reaction is proportional to the amount of Pd^{2+} in Pd/H-ZSM-5 [27]. They proposed that the Pd^{2+} species in ZSM–5facilitates the NO$_2$–CH$_4$–O$_2$ reaction by providing NO adsorption sites, and this is consistent with the present results [27].

After exchanging the ionic-Pd species of the Pd(2)/ZSM-5 (30) 500C and 750C with NH$_4$NO$_3$, the catalysts were reoxidized at 750 °C to evaluate their NO adsorption capability. As displayed in Fig. 5, a slight NO amount was adsorbed on the catalyst of the Pd(2)/ZSM-5 750C after the ion exchange with NH$_4$NO$_3$, while an appreciable amount of NO was adsorbed on the catalyst of the Pd(2)/ZSM–5 500C, which was
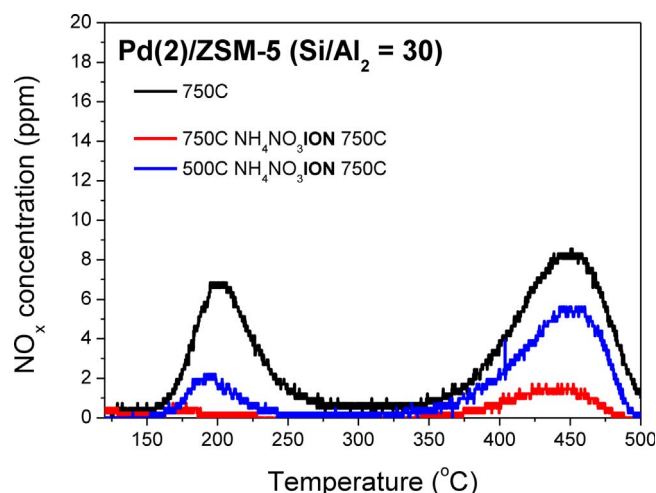
ion-exchanged with the NH$_4$NO$_3$; this was followed by the treatment at 750 °C, as most of the Pd species survived after the titration. The 2.6 μmol/g$_{catal}$ of NO that was adsorbed on the former and the 11.4 μmol/g$_{catal}$ that was adsorbed on the latter correspond to 10% and 46% of the NO adsorption ability of the initial Pd(2)/ZSM–5 750C catalyst, respectively. It is likely that the residual bulk-PdO species on the catalyst of the Pd(2)/ZSM–5 500C were redispersed by the subsequent oxidative treatment at 750 °C. A proportional relationship was observed between the amount of Pd that was ion-exchanged from the Pd/ZSM–5 and the extent of the deterioration of the NO adsorption capability; when 79% (44%) of Pd was ion-exchanged with the NH$_4$NO$_3$, 90% (54%) of the NO adsorption ability was lost. It became obvious that when the ionic-Pd species, which are the active NO adsorption sites at low temperatures, are ion-exchanged with NH$_4$NO$_3$, the NO adsorption ability proceeds to deteriorate.

3.2. The effect of the Si/Al$_2$ ratio and Pd loading on the NO adsorption ability of the Pd/ZSM–5

Fig. S5 presents the ICP-AES results of the Pd/ZSM–5 catalysts. Here, 0.1 g of Pd(NO$_3$)$_2$(H$_2$O)$_2$ was dissolved in DIW and ion-exchanged into 2 g of NH$_4$-ZSM-5. The amount of Pd that was dissolved in the DIW was fixed to observe whether the SARs of the ZSM–5 influence the easiness of the Pd ion exchange. For the ZSM–5 with the SARs of 23, 30,

50 and 80, most of the Pd species that had been dissolved in the DIW were successfully loaded, resulting in a linear relationship between the Si/Al$_2$ and Pd/Al ratios. However, on the ZSM–5 with the SAR of ~300, only half of the Pd nitrate that had been dissolved in the DIW was ion-exchanged, resulting in a Pd-to-Al molar ratio of 1. If all of the Pd nitrate that had been dissolved in the DIW was successfully ion-exchanged into the ZSM–5 (300), as it did on the ZSM–5 with the lower SARs (23, 30, 50 and 80), a Pd/Al ratio of 2 instead of 1 would have been the result. It is obvious that the lack of Al on the ZSM–5 with the SAR of ~300 restricted the amount of Pd species that was loaded into the ZSM–5. In addition, the Pd-to-Al molar ratio of 1 indicates that the amount of Al on the ZSM–5 (300) imposes a Pd-loading upper limit.

Since Fig. 1 showed that the NO adsorption ability of Pd/ZSM-5 was activated after the oxidative treatment at 750 °C, all of the characterization studies were performed after the oxidative treatment at 750 °C. It should be emphasized that all of the prepared catalysts in the present work showed a superior NO adsorption ability after the oxidation at 750 °C. It is interesting to note that even though the Pd was loaded on the ZSM–5 by the ion-exchange method, a high thermal-energy value is required for the Pd species to migrate to the ionic sites so that an effective NO adsorption capability can be attained.

Fig. 6 shows the XRD patterns of the catalyst of the Pd/ZSM-5 750C. The Pd/ZSM-5 catalysts showed XRD patterns that are characteristic of the ZSM–5 structure as demonstrated in Fig. 6 (a). In Fig. 6 (b), the 2θ region between 31 and 37° was finely scanned to observe the XRD peaks of the bulk-PdO phase at the 2θ region between 33.5 and 33.8°. The Pd/ZSM–5 with the SAR of 80 showed the highest XRD-peak intensity from the bulk PdO, while those with the SARs of 23 and 30 did not show XRD peaks for the bulk-PdO phase. The Pd/ZSM–5 with the SARs of 50 and ~300 also showed XRD peaks for the bulk-PdO phase, but their intensity values are lesser than that from a SAR of 80. The weak PdO peak in the XRD pattern of the Pd/ZSM–5 (300) can be attributed to the low Pd loading (1 wt%) as shown in Table 1. Similar trends were observed on the Raman spectra of the Pd/ZSM–5 catalysts after the oxidative treatment at 750 °C (Fig. S6). According to Weber et al., the Raman band at 650 cm^{-1} originates from the bulk PdO [37]. More intense bulk-PdO Raman bands were observed on the Pd/ZSM–5 catalysts with the SARs of 50, 80 and ~300 compared with the samples with SARs of 23 and 30. In agreement with the XRD results, the Pd/ZSM–5 with the SAR of 80 showed the most intense Raman band from the bulk PdO. Both the XRD patterns (Fig. 6) and the Raman spectra (Fig. S6) indicate that the Pd species on the ZSM–5 with a low Al content tend to aggregate into the bulk PdO more significantly.

Fig. 7(a) shows the NO$_x$ desorption curves of the catalyst of the Pd (2)/ZSM–5 750C with different SARs (see Table 1). On the Pd/ZSM–5 with the SARs of 50, 80 and ~300 (Al/Si of 0.007, 0.025 and 0.040, respectively), the NO$_x$ was desorbed only at the temperatures above 300 °C with a desorbed-NO$_x$ amount that is less than 0.3 μmol. Alternatively, two NO$_x$ desorption peaks were observed on the Pd/ZSM–5 with the SARs of 23 and 30 (Al/Si ratios of 0.087 and 0.067, respectively), where the first and second peaks are centered at 200 and 450 °C, respectively. The NO$_x$ amounts that were desorbed at low and high temperatures are marked on Fig. 7(b). The total NO$_x$ amount that was desorbed from the Pd/ZSM–5 with the SARs of 23 and 30 are 0.55 and 0.86 μmol, respectively, and these are higher than those from the Pd/ZSM–5 with the SARs of 50, 80 and ~300. Among the Pd/ZSM-5 catalysts, the Pd/ZSM–5 with the SAR of 30 has the largest NO adsorbed amount as shown in Fig. 7(b). More specifically, the amount of NO$_x$ that was desorbed below 300 °C is similar between the Pd/ZSM–5 with the SARs of 23 and 30; however, the Pd/ZSM–5 with the SAR of 30 showed the largest amount of desorbed NO$_x$ above 300 °C. Interestingly, the NO$_x$ desorption peak below 300 °C was detected only on the Pd/ZSM-5 with the SARs of 23 and 30, where the bulk-PdO species are not evident on the XRD pattern (Fig. 6). It appears that the presence of the bulk PdO is detrimental to the NO adsorption ability.

To investigate the optimum Pd loading on the ZSM–5 with the SAR of 30 with respect to the NO adsorption ability, different Pd amounts were ion-exchanged (see Table 1). For the NO adsorption test, 0.5, 1, 2, 3 and 6 wt% of Pd were ion-exchanged into the ZSM–5 with the SAR of 30 and oxidized at 750 °C. Fig. 8(a) shows the corresponding NO$_x$ desorption curves. The amounts of NO$_x$ that were desorbed below and above 300 °C are shown as a function of the Pd loading in Fig. 8(b). With the Pd loading of 0.5 wt%, only a NO$_x$ desorption peak that is centered at 470 °C was observed. When the Pd loading was raised to 1 wt%, another NO$_x$ desorption peak appeared at 200 °C, while the intensity of the high-temperature peak was increased. At a Pd loading of 2 wt%, the intensities of both the low- and high-temperature peaks were increased, and the high-temperature peak shifted to a lower temperature with its maximum peak observed at 450 °C. When the Pd loading was further raised to 3 and 6 wt%, the NO adsorption capability of the Pd/ZSM–5 (30) was greatly decreased. The integrated amount of NO$_x$ that was desorbed at ~200 °C was decreased to 6.6 and 0.6 μmol/g$_{catal}$ when 3 and 6 wt% of Pd were loaded, respectively. The intensity of the high-temperature peak also dwindled with the shift of its peak maximum to 370 °C. For the best NO adsorption ability, the optimum Pd loading on the ZSM–5 with the SAR of 30 is 2 wt%, where the largest NO$_x$ desorption peaks were obtained at both the low- and high-temperature regimes. The Pd loading was also varied on the ZSM–5 with the SARs of 50 and 23, and the NO adsorption ability was evaluated. As displayed in Table 1 and Fig. S7, the optimum Pd loading for the NO
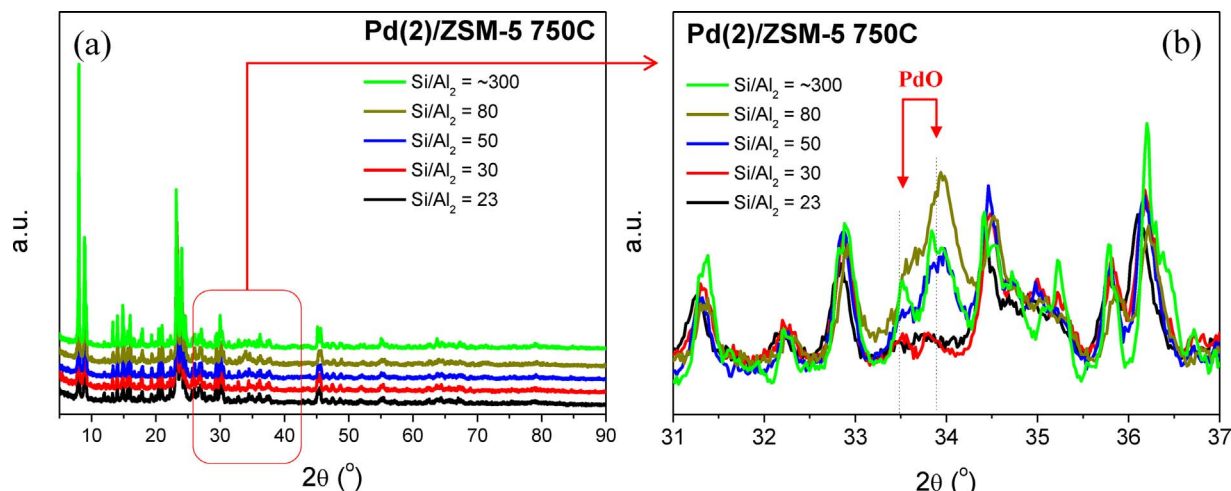

Fig. 6. X-ray diffraction (XRD) patterns of the Pd(2)/ZSM–5 750C catalyst with different Si/Al$_2$ ratios, (a) a wide scan in the 2θ region of 5–90° and (b) a fine scan in the 2θ region of 31–37°.
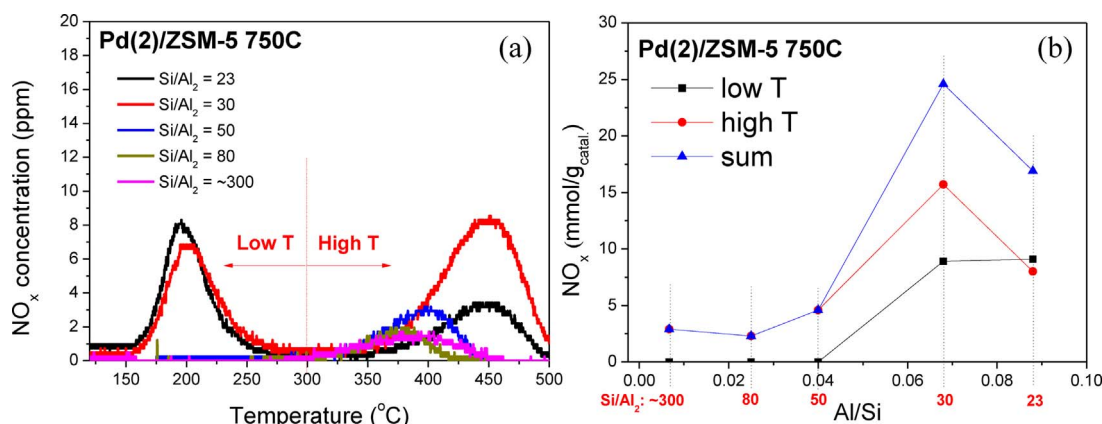
Fig. 7. (a) NO$_x$ desorption curves of the Pd(2)/ZSM–5 750C catalyst with different Si/Al$_2$ ratios. The amounts of NO$_x$ that were desorbed below and above 300 °C were integrated separately and marked on (b).

adsorption is 1 wt% on the ZSM–5 (50) and 3 wt% on the ZSM–5 (23), thereby implying that the optimum Pd loading depended strongly on the SARs of the ZSM–5. The present research is in partial agreement with the previous results of Murata et al., who observed that 1 wt% of Pd saturated the NO adsorption ability of the Pd/ZSM–5 with a SAR of 50 [32]. Contrary to their result, however, the increase of the Pd loading above the optimum value did not saturate but decreased the NO adsorption ability of the Pd/ZSM–5 catalysts in the present work. The same pattern was observed for the Pd/ZSM–5 with the SARs of 23, 30 and 50.

Fig. 9(a) demonstrates the XRD patterns of the Pd/ZSM–5 (30) with different Pd loadings. The 2θ region between 31 and 37° was fine-scanned and is magnified in Fig. 9(b) for the observation of the XRD-peak evolution from the bulk-PdO phase (33.5 and 33.8°) at a higher resolution. At the Pd loading of 6 wt%, appreciable XRD peaks of the bulk-PdO phase were observed as shown in Fig. 9(a). Even at the Pd loading of 3 wt%, the evolution of the XRD peak from the bulk-PdO phase is evident in the XRD pattern of Fig. 9(b). The formation of the bulk-PdO cluster seems detrimental to the NO adsorption ability, since the NO adsorption capabilities of the Pd/ZSM–5 with the Pd loadings of 3 and 6 wt% (12.9 and 6.0 μmol/g$_{catal}$) are much less than that of the Pd/ZSM–5 with the Pd loading of 2 wt% (24.6 μmol/g$_{catal}$) as shown in Fig. 8.

Fig. 10 shows the H$_2$-TPR spectra of the Pd/ZSM–5 (23, 30) catalysts with various Pd loadings. When 1-wt% Pd was loaded on the ZSM–5 (30), a broad reduction peak from 50 to 150 °C was observed without a large H$_2$-consumption peak at around 0 °C, which could be attributed to

the dominant existence of the ionic-Pd species [35]. When the Pd loading was increased to 2 wt%, the reduction peak of the ionic Pd was intensified with the appearance of a small additional peak at ~20 °C, which is attributed to the reduction of the PdO bulk [35]. When the Pd loading was further raised to 3 wt%, the reduction peak of the bulk PdO at 20 °C became the dominant feature, and the hydride-decomposition peak was also observed at ~70 °C. For a comparison, the H$_2$-TPR spectrum of the Pd(1)/Al$_2$O$_3$ 500C, that is also presented in Fig. 10 (a), demonstrates the typical reduction of the PdO followed by the PdH$_x$ decomposition. In agreement with the XRD results of Fig. 9, the H$_2$-TPR spectra in Fig. 10 (a) also show that the Pd loading of 3 wt% on the ZSM–5 (30) led to the formation of the bulk PdO. A similar trend was observed on the H$_2$-TPR spectra of the Pd/ZSM-5 (23) 750C as shown in Fig. 10 (b); when the Pd loading was increased from 3 to 4 wt%, the reduction peak from the bulk PdO became dominant. Since the optimum Pd loadings are 2 and 3 wt% on the ZSM–5 (30) and (23) in Fig. 8 and Fig. S7, respectively, it could be concluded that the formation of the bulk-PdO species, and therefore the NO adsorption capability, is strongly dependent on the SAR of the ZSM–5.

Fig. 11 shows the NH$_3$-TPD curves of the Pd/ZSM–5 (30) with different Pd-loading amounts. The ZSM–5 (30) 750C showed two NH$_3$ desorption peaks at ~220 and ~420 °C. According to the references [38–40], the low- and high-temperature peaks can be attributed to the desorption of weakly bound NH$_3$ and the Bronsted acid sites bound with NH$_3$, respectively. When a 1-wt% Pd was loaded, the NH$_3$ desorption peak at ~220 °C was decreased while the intensity of the NH$_3$ desorption peak at ~400 °C was increased. In addition, a sharp desorption
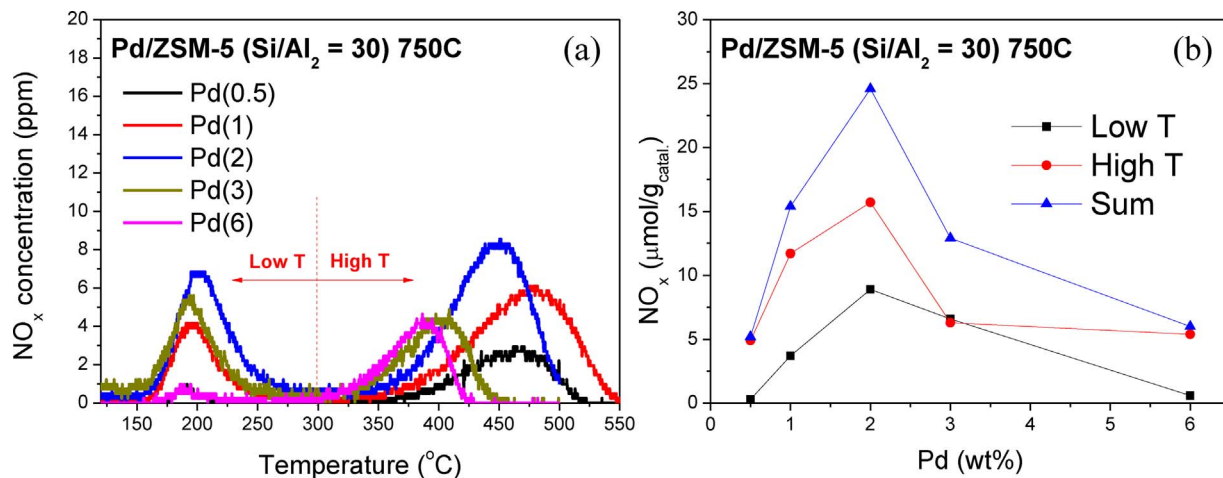

Fig. 8. (a) NO$_x$ desorption curves of the Pd/ZSM–5 (Si/Al$_2$ = 30) 750C catalyst with different Pd loadings (wt%). The amounts of NO$_x$ that were desorbed below and above 300 °C were integrated separately and are marked on (b).
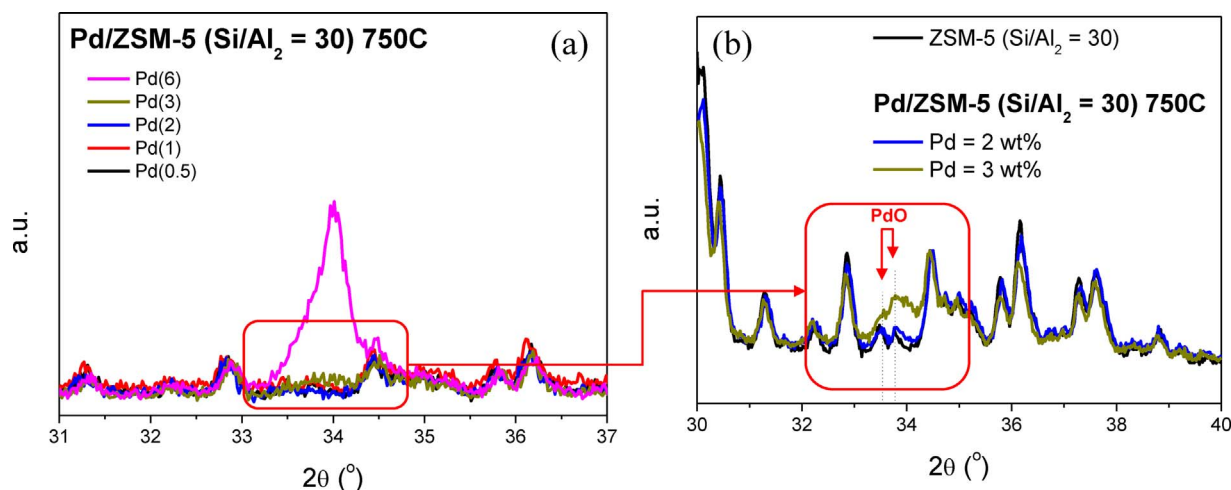
Fig. 9. X-ray diffraction (XRD) patterns of the Pd/ZSM-5 (Si/Al$_2$ = 30) 750C catalyst with different Pd loadings (wt%), (a) in the 2θ region of 31–37° and (b) a fine scan of selected catalysts in the 2θ region of 30–40°.

peak was observed at ~ 371 °C as can be seen in Fig. 11 (a). When the Pd loading was increased to 2 wt%, the NH$_3$ desorption peak at 220 °C was further decreased, while the peak intensity at 400 °C was increased. A sharp desorption peak was also observed, and moreover, it shifted to the lower temperature at 353 °C, which is also shown in Fig. 11 (a). When the Pd loading was raised to 3 wt%, the NH$_3$ desorption peaks at 220 and 430 °C were not affected, but only the sharp desorption peak was shifted to the lower temperature at 305 °C, and this is shown in Fig. 11 (b). In summary, the presence of Pd in the ZSM–5facilitates the development of a broad NH$_3$ desorption peak at around 400 °C as well as a sharp NH$_3$ desorption peak in the temperature region of 305–371 °C.

To investigate the origin of the sharp desorption peak, the NH$_3$-TPD curve of the Pd(2)/Al$_2$O$_3$ 500C was plotted together with those of the Pd/ZSM-5 750C catalysts with Pd loadings of 1, 2 and 3 wt% as shown in Fig. 11(b). The Pd dispersion of the Pd(2)/Al$_2$O$_3$ 500C was estimated as 7% according to the CO chemisorption, and the Pd species existed in the PdO phase according to the XPS, TEM and XRD experiments (data not shown). It is shown in Fig. 11(b) that the bulk PdO on the Al$_2$O$_3$ gave rise to the sharp desorption peak at 280 °C, which was not observed in the absence of Pd (Fig. S8). Therefore, the sharp desorption peak could be ascribed to the NH$_3$ that had adsorbed on the PdO species. At the low Pd-loading values (1 and 2 wt%), the sharp desorption peaks were observed at 371 and 353 °C, respectively. However, when a

3-wt% Pd was loaded on the ZSM–5, where the evolution of the bulk PdO was detected from the XRD and H$_2$-TPR analyses as shown in Figs. 9 and 10, respectively, the sharp desorption peak was observed at a temperature that is slightly higher than that of the Pd(2)/Al$_2$O$_3$ 500C. It seems reasonable to suggest that the formation of the large PdO clusters on the Pd(3)/ZSM–5 (30) lowered the desorption temperature of the sharp peak. Fig. 11 shows that the Pd species on the ZSM–5 might exist in two different states as follows: First, the Pd^{2+} that gave rise to the desorption peak at around 400 °C, since the intensity of the NH$_3$ desorption peak at ~ 400 °C was increased after the Pd loading, and secondly, the PdO that caused the sharp NH$_3$ desorption peak in the temperature region of 300–370 °C.

4. Discussion

4.1. Role of the interaction between the ZSM–5 Al and Pd in the NO adsorption capability

The catalysts of the Pd/ZSM–5 750C with the SARs of 23 and 30 showed a superior NO adsorption ability in this study compared with those of the Pd/ZSM–5 750C with the SARs of 50, 80 and ~ 300. In addition, the formation of the bulk PdO was suppressed on the Pd/ZSM–5 750C with the SARs of 23 and 30. The high Al concentration in the ZSM–5 suppressed the Pd sintering and promoted the NO
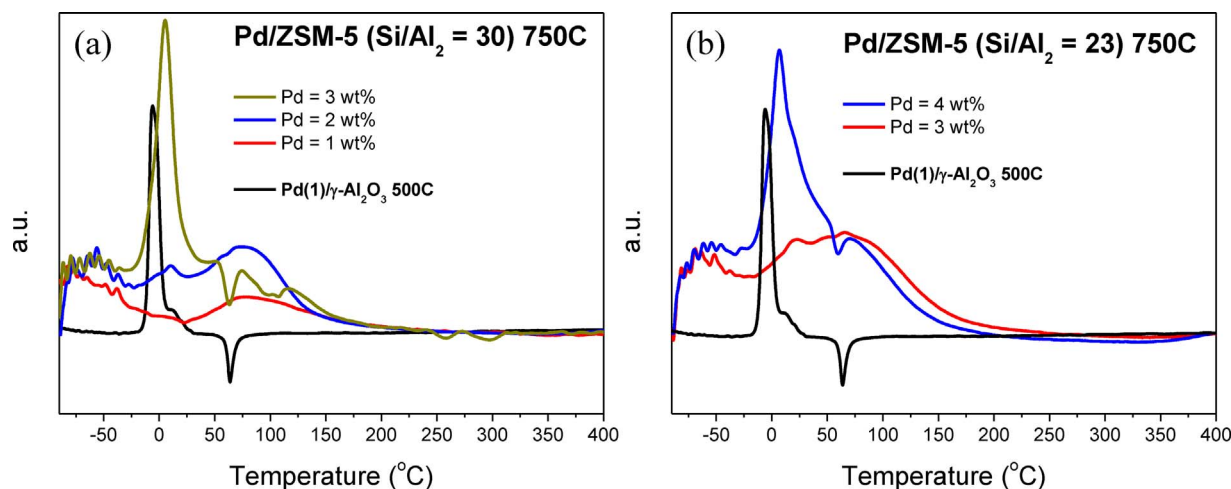

Fig. 10. Cryo-H$_2$-TPR curves of the (a) Pd/ZSM–5 (Si/Al$_2$ = 30) 750C and (b) Pd/ZSM–5 (Si/Al$_2$ = 23) 750C catalysts with different Pd loadings (wt%). Cryo-H$_2$-TPR curve of the Pd(1)/γ-Al$_2$O$_3$ 500C is also provided as a reference.
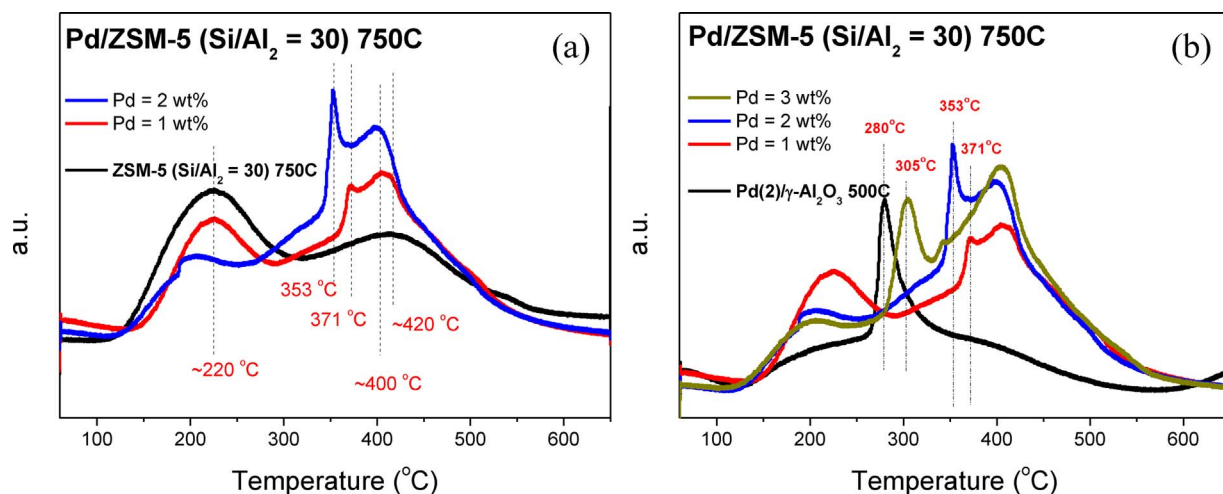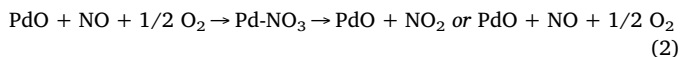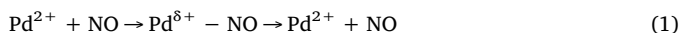
Fig. 11. (a) NH$_3$-TPD curves of the Pd(1, 2)/ZSM–5 (Si/Al$_2$ = 30) 750C and ZSM–5 (Si/Al$_2$ = 30) 750C catalysts. (b) NH$_3$-TPD curves of the Pd/ZSM–5 (Si/Al$_2$ = 30) 750C catalyst with different Pd loadings (1, 2 and 3 wt%) and the Pd(2)/γ-Al$_2$O$_3$ 500C catalyst that is provided as a reference.

adsorption at the low temperature. Therefore, the interaction between the Pd and the Al would be the critical factor in the determination of the thermal stability of the Pd and the NO adsorption ability of the Pd/ZSM–5 catalysts. The optimum Pd loadings for the NO adsorption ability are 3, 2 and 1 wt% on the ZSM–5 with the SARs of 23, 30 and 50, respectively; that is, the higher the Al concentration on the ZSM–5, the higher the optimum Pd loading. Interestingly, the Pd/Al ratio of the optimized catalysts are very close to each other; 0.26 and 0.24 on the Pd/ZSM–5 with the SARs of 23 and 30, respectively. This finding indicates the existence of certain Al species on the ZSM–5 that can interact with Pd to activate the NO adsorption capability. Rice et al. [41] previously reported that the maximum values of M^{2+}/Al and [M-O-M]$^{2+}$/Al are 0.12 and 0.3 for the ZSM–5 with a SAR of 24, respectively, based on their Monte-Carlo simulation results for which they adopted Lowenstein's rule. They also suggested that at high SARs for which the Poisson distribution of the Al species is assumed, the probability of the Al–Al pair is decreased exponentially [41]. If the Al-distribution model that was proposed by Rice et al. [41] is adopted, the Pd species on the ZSM–5 should be balanced by the two Al sites to adsorb NO. Presently, the optimum Pd/Al ratio for the NO adsorption exists at ~0.25 on the ZSM–5 with the SARs of 23 and 30. In addition, the Pd/ZSM–5 catalysts with a high SAR (≥50) that represents a low Al concentration, for which paired low-Al site concentrations are also assumed, exhibited a poor NO adsorption ability. Therefore, the present results seem to be in reasonable agreement with the proposed model of Rice et al. Also, regarding their Cu/ZSM–5 catalysts (SAR of 28), Wichterlova et al. reported that Cu$_\alpha$/Al, where the Cu is balanced by two Al sites, converges to around 0.25 as the Cu loading is increased [42], which is close to the obtained optimum Pd/Al ratio of the current results. In addition, Aylor used their calibration results to suggest that, in association with pairs of next-nearest-neighbor Al sites, the highly stabilized isolated-Pd species in the ZSM–5 may reside as Al$^-$H$^+$(PdO)H$^+$Al$^-$ [31]. To summarize, it appears that paired Al sites are necessary on the ZSM–5 to stabilize the isolated-Pd species and to activate the NO adsorption capability. On the ZSM–5 with higher Al concentrations, the larger amount of paired Al species would require higher Pd concentrations to reach the optimum NO adsorption capability thereby leading to a Pd/Al of ~0.25. In addition, above the optimal Pd loading, the Pd sintering that is evident in the XRD pattern of Fig. 9 will occur thereby explaining the decrease of the NO adsorption capability at high Pd loadings that can be seen in Fig. 8.

4.2. Active Pd species on the ZSM–5 for the NO adsorption at the low temperature

Fig. 2 shows the NO and NO$_2$ desorption profiles of the catalyst of the Pd(2)/ZSM–5 (30) 750C. The NO$_x$ desorption peak below 300 °C consists of an almost-1:1 ratio of NO and NO$_2$, while the NO$_x$ desorption peak above 300 °C mainly consists of NO. This finding implies the existence of at least two different Pd species that are capable of adsorbing NO at 120 °C. Previously, Chen et al. investigated the differences in the behavior of the nitrate formation between the Cu/CHA and Cu/BEA catalysts [43]. They found that when the catalysts are exposed to NO and O$_2$, stable nitrates formed on only the Cu/BEA and not on the Cu/CHA. The difference here is attributed to the existence of extra-lattice oxygen (ELO) on the Cu/BEA, as it facilitates the nitrate formation, whereas this cannot be enacted by the isolated Cu cations in the Cu/CHA [43]. Analogous to their suggested model, extra oxygen (O) should be required for the evolution of NO$_2$ in the NO$_x$ desorption profile below 300 °C. The NH$_3$-TPD curves of Fig. 11 suggest that the Pd species in the ZSM–5 exist as the PdO or Pd^{2+} states, which might be responsible for the NO$_x$ desorption curves below and above 300 °C, respectively. The extra O of the isolated PdO would facilitate the adsorption of NO in a nitrate-like form, while the Pd^{2+} would adsorb the NO in a nitrosyl-like form. In agreement with the present proposal, Pommier and Gelin also observed the evolution of NO$_2$ on the Pd/ZSM–5 during the NO$_x$ desorption process [44]. Since they carried out the NO adsorption in the absence of O$_2$, they suggested that the NO$_2$ was produced by the reaction of NO with the O that is bound on the Pd species [44,45].

A number of controversies have arisen over the chemical states of the Pd species in the ZSM–5. Adelman et al. suggested that the Pd^{2+} species are formed by the reaction of the isolated-PdO species with the H of the ZSM–5 [35], while Aylor et al. proposed that the isolated-PdO species are stabilized by the paired Al sites in the ZSM–5 [31]. Possibly, the Pd^{2+} and the isolated-PdO species would coexist in the ZSM–5, which is also supported by the NH$_3$-TPD data as shown in Fig. 11. It should be noted that these Pd^{2+} or isolated-PdO species would be hydrated in the presence of H$_2$O resulting in the formation of Pd(H$_2$O)$_x$ or Pd(OH)$_2$ species [45–47]. The hydrated ionic-Pd species would be able to perform the ion exchange with the other cations as has been addressed in Table 4. The interaction between the Pd species and H$_2$O could be complicated as has been pointed out by several authors, and further investigation is required [45,46]. In summary, a possible interaction between the Pd^{2+} and PdO species and NO may result in adsorption as follows:

$$Pd^{2+} + NO \rightarrow Pd^{\delta+} - NO \rightarrow Pd^{2+} + NO \quad (1)$$

$$PdO + NO + 1/2\ O_2 \rightarrow Pd\text{-}NO_3 \rightarrow PdO + NO_2\ or\ PdO + NO + 1/2\ O_2 \quad (2)$$

Recently, Yang et al. drew similar conclusions based on their CO-diffuse reflectance infrared Fourier transform (DRIFT) and in situ XPS results as follows: Naked Pd^{2+} ions in zeolite chemisorb NO into a nitrosyl form, while the palladium hydroxide (PdOH) species in zeolite transform NO into NO_2 during the NO-chemisorption processes [48]. Thus, it can be concluded that the Pd species will exist in two different chemical states for the NO chemisorption in the ZSM–5.

Aylor et al. previously reported that when Pd/ZSM–5 was reduced by CO, the Pd species were aggregated to fill the pores of the ZSM–5 [31]. Sachtler et al. also reported that the CO chemisorption increased the mobility of the Pd species in zeolite resulting in the agglomeration of the Pd [49,50]. It is expected that, if the Pd species in the ZSM–5 exist in different environments, they may respond differently to the CO treatment. It has also been reported that the PdH_x species that are formed by the reaction between the larger Pd particles and hydrogen are more stable against the thermal treatment and decompose at a higher temperature. For example, Nag et al. [51] reported on their Temperature-Programmed study wherein the PdH_x phase that formed on the larger Pd crystallite decomposed at a higher temperature. Bonarowska et al. [52] also investigated the hydride-formation/decomposition behavior of the Pd–gold (Au)/SiO_2 catalyst using the TPHD technique. They observed that, when Pd particles are bimodally distributed on SiO_2, the PdH_x on the well-dispersed Pd particles gives rise to the decomposition peak at a lower temperature compared with the PdH_x on the large Pd particles.

It is expected that if the CO treatment induces Pd agglomeration to a different extent depending on the chemical state of the Pd species, the hydride-formation/decomposition behavior of the Pd particles after the CO treatment would provide indirect evidence about the different chemical states of the Pd species in the ZSM–5. Fig. 12 displays the TPHD curves of the catalysts of the Pd(2)/ZSM–5 (30 and ~300) 750C after the CO treatment at 300 °C that was followed by an N_2 treatment at 400 °C. Two PdH_x-decomposition peaks were observed at 43 and 68 °C on the Pd(2)/ZSM–5 (30) 750C, while only one peak with a lower intensity was observed at 68 °C on the Pd(2)/ZSM–5 (300) 750C. For a
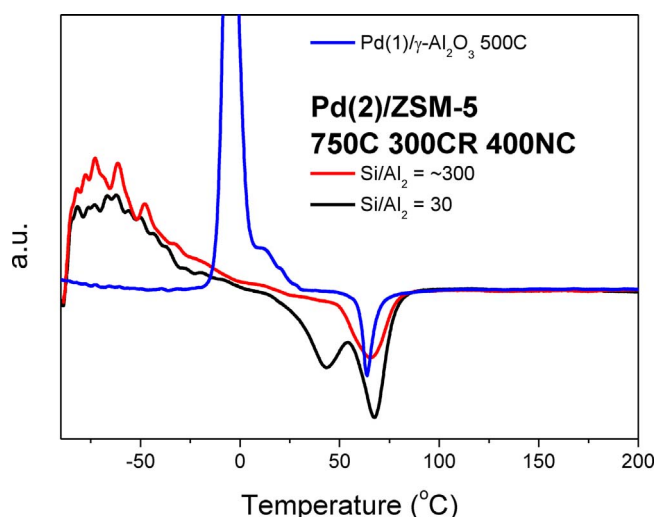

Fig. 12. Temperature-programmed hydride decomposition (TPHD) curves of the Pd(2)/ZSM–5 with Si/Al_2 ratios of 30 and ~300. After the oxidative pretreatment at 750 °C, the catalysts were treated under a CO flow at 300 °C followed by an N_2 treatment at 400 °C to remove the adsorbed CO from the Pd. After the cooling of the sample temperature down to −90 °C, the catalysts were stabilized under a H_2 flow for 30 min, and the temperature was ramped under the H_2 flow. For a comparison, the H_2-TPR curve of the Pd(1)/γ-Al_2O_3 500C catalyst is also provided in the figure.

comparison, the H_2-TPR curve of the Pd(1)/Al_2O_3 500C is plotted in Fig. 12, where the hydride-decomposition peak is evident at 63 °C. The two PdH_x-decomposition peaks of the Pd(2)/ZSM–5 (30) at 43 and 68 °C should originate from small and large Pd crystallites, respectively, as this means that the Pd species exist in two different chemical states on the ZSM–5 (30) as suggested previously in Fig. 2, and these should respond differently to the CO treatment. It is likely that the Pd^{2+} cations, rather than the isolated PdO, would interact more weakly with CO gas giving rise to the decomposition peak at 43 °C, because an O source that is needed for a conversion of the CO into CO_2 is absent. Alternatively, the Pd species on the ZSM–5 (300) exist mainly in the bulk-PdO phase because of the low Al concentration (Fig. 6 and Table 4). Therefore, the decomposition peaks of the PdH_x species on the ZSM–5 (300) and the gamma (γ)-Al_2O_3 were observed at the similar temperatures of 68 and 63 °C, respectively. In summary, regarding NO adsorption, the TPHD curves in Fig. 12 provide indirect evidence about the presence of the active-Pd species of two different chemical states on the ZSM–5; one is the Pd^{2+} species and the other is the isolated-PdO species. After the CO treatment, the PdO species seemed to form larger Pd agglomerates compared with the Pd^{2+} species giving rise to the PdH_x-decomposition peak at the higher temperature.

5. Conclusion

The NO adsorption ability of Pd/ZSM–5 was investigated as a function of the treatment condition, Pd loading and SARs of the ZSM–5. The Pd/ZSM–5 showed a superior NO adsorption ability after an oxidative treatment at 750 °C. According to the EXAFS, XPS and XRD results, atomically dispersed Pd species were formed on the Pd/ZSM–5 (30) after an oxidation at 750 °C, while small Pd agglomerates were observed after an oxidation at 500 °C. It can be claimed that the oxidative treatment at 750 °C induced the redispersion of the Pd on the ZSM–5. The NO adsorption sites on the Pd/ZSM–5 were further investigated using a NH_4NO_3-titration method, which allowed the ion exchange of only the ionic-Pd species. When the Pd(2)/ZSM–5 (30) 750C was ion-exchanged with NH_4NO_3, 79% of the Pd was ion-exchanged and the catalyst lost much of its NO adsorption capability. Alternatively, a smaller amount of Pd was ion-exchanged on the Pd/ZSM–5 with a low NO adsorption capability. It could be concluded that the ionic-Pd species on the ZSM–5 are the active sites for the adsorption of NO at low temperatures.

To investigate the influences of the Pd loading and the SAR of the ZSM–5 on the NO adsorption ability of the Pd/ZSM–5, various Pd/ZSM–5 samples with different Pd loadings and SARs were prepared. It became evident that the high Al concentration on the Pd/ZSM–5 provided a high NO adsorption ability. A high Al concentration on the Pd/ZSM–5 also suppressed the PdO sintering, while the presence of the bulk-PdO phase hindered the NO adsorption ability of the Pd/ZSM–5 catalysts. The optimum Pd-to-Al molar ratio for the maximum NO adsorption ability was found at around 0.25. Above the optimum Pd loading, the bulk-PdO phase formed in the ZSM–5 and the NO chemisorption ability was deteriorated. Therefore, it can be summarized that the Al concentration of the ZSM–5 significantly influences the interaction between the Pd and ZSM–5 and the NO adsorption ability. Among the catalysts that were investigated, the Pd(2)/ZSM–5 with the SAR of 30 showed the best NO_x storage performance.

Acknowledgments

Appendix A. Supplementary data

Supplementary data associated with this article can be found, in the online version, at https://doi.org/10.1016/j.apcatb.2017.12.031.

References

[1] R.M. Heck, R.J. Farrauto, S.T. Gulati, Catalytic Air Pollution Control: Commercial Technology, John Wiley & Sons, 2009.

[2] J.H. Kwak, D.H. Kim, J. Szanyi, C.H. Peden, Appl. Catal. B Environ. 84 (2008) 545–551.

[3] D.H. Kim, K. Mudiyanselage, J. Szanyi, J.H. Kwak, H. Zhu, C.H. Peden, Appl. Catal. B Environ. 142 (2013) 472–478.

[4] I. Song, S. Youn, D.H. Kim, Top. Catal. (2016) 1–5.

[5] S.G. Lee, H.J. Lee, I. Song, S. Youn, D.H. Kim, S.J. Cho, Sci. Rep. 5 (2015), http://dx.doi.org/10.1038/srep12702.

[6] L. Ma, Y. Cheng, G. Cavataio, R.W. McCabe, L. Fu, J. Li, Appl. Catal. B Environ. 156 (2014) 428–437.

[7] J.H. Kwak, R.G. Tonkyn, D.H. Kim, J. Szanyi, C.H. Peden, J. Catal. 275 (2010) 187–190.

[8] S.D. Yim, S.J. Kim, J.H. Baik, I.S. Nam, Y.S. Mok, J.-H. Lee, B.K. Cho, S.H. Oh, Ind. Eng. Chem. Res. 43 (2004) 4856–4863.

[9] I. Song, S. Youn, H. Lee, D.H. Kim, Korean J. Chem. Eng. 33 (2016) 2547–2554.

[10] K. Zhang, L. Xu, S. Niu, C. Lu, D. Wang, Q. Zhang, J. Li, Korean J. Chem. Eng. (2017) 1–9.

[11] T.V. Johnson, SAE Paper 5 (2012) 216–234.

[12] H.-Y. Chen, S. Mulla, E. Weigert, K. Camm, T. Ballinger, J. Cox, P. Blakeman, SAE Int. J. Fuels Lubr. 6 (2013) 372–381.

[13] F. Millo, D. Vezza, SAE Paper (2012), http://dx.doi.org/10.4271/2012-01-0373.

[14] H.-Y. Chen, J.E. Collier, D. Liu, L. Mantarosie, D. Durán-Martín, V. Novák, R.R. Rajaram, D. Thompsett, Catal. Lett. 146 (2016) 1706–1711.

[15] H.-Y. Chen, S. Mulla, U.S. Patent US20120308439 A1, (2011).

[16] R.R. Rajaram, F.-M. McKENNA, H.-Y. Chen, D. Liu, U.S. Patent US20150157982 A1, (2014).

[17] F.-M. McKENNA, U.S. Patent US20130287658 A1, (2015).

[18] A. Vu, J. Luo, J. Li, W.S. Epling, Catal. Lett. 147 (2017) 745–750.

[19] Y. Ryou, J. Lee, S.J. Cho, H. Lee, C.H. Kim, D.H. Kim, Appl. Catal. B Environ. 212 (2017) 140–149.

[20] T.J. Lee, I.-S. Nam, S.-W. Ham, Y.-S. Baek, K.-H. Shin, Appl. Catal. B Environ. 41 (2003) 115–127.

[21] M.H. Kim, I.-S. Nam, Korean J. Chem. Eng. 18 (2001) 725–740.

[22] Y. Nishizaka, M. Misono, Chem. Lett. (1994) 2237–2240.

[23] C.J. Loughran, D.E. Resasco, Appl. Catal. B Environ. 5 (1995) 351–365.

[24] C.J. Loughran, D.E. Resasco, Appl. Catal. B Environ. 7 (1995) 113–126.

[25] G. Koyano, S. Yokoyama, M. Misono, Appl. Catal. A Gen. 188 (1999) 301–312.

[26] A. Ali, W. Alvarez, C. Loughran, D. Resasco, Appl. Catal. B Environ. 14 (1997) 13–22.

[27] M. Ogura, M. Hayashi, S. Kage, M. Matsukata, E. Kikuchi, Appl. Catal. B Environ. 23 (1999) 247–257.

[28] M. Ogura, S. Kage, M. Hayashi, M. Matsukata, E. Kikuchi, Appl. Catal. B Environ. 27 (2000) L213–L216.

[29] H. Ohtsuka, T. Tabata, Appl. Catal. B Environ. 26 (2000) 275–284.

[30] K. Okumura, J. Amano, N. Yasunobu, M. Niwa, J. Phys. Chem. B 104 (2000) 1050–1057.

[31] A.W. Aylor, L.J. Lobree, J.A. Reimer, A.T. Bell, J. Catal. 172 (1997) 453–462.

[32] Y. Murata, T. Morita, K. Wada, H. Ohno, SAE Int. J. Fuels Lubr. 8 (2015) 454–459.

[33] J. Chastain, R.C. King, J. Moulder, Handbook of X-ray Photoelectron Spectroscopy: A Reference Book of Standard Spectra for Identification and Interpretation of XPS Data, Physical Electronics Eden Prairie, MN, 1995.

[34] B. Ravel, M. Newville, J. Synchrotron Radiat. 12 (2005) 537–541.

[35] B. Adelman, W. Sachtler, Appl. Catal. B Environ. 14 (1997) 1–11.

[36] L. Wang, J.R. Gaudet, W. Li, D. Weng, J. Catal. 306 (2013) 68–77.

[37] W. Weber, R. Baird, G. Graham, J. Raman Spectrosc. 19 (1988) 239–244.

[38] N. Katada, H. Igi, J.-H. Kim, M. Niwa, J. Phys. Chem. B 101 (1997) 5969–5977.

[39] F. Lónyi, J. Valyon, Micropor. Mesopor. Mater. 47 (2001) 293–301.

[40] L. Rodríguez-González, F. Hermes, M. Bertmer, E. Rodríguez-Castellón, A. Jiménez-López, U. Simon, Appl. Catal. A Gen. 328 (2007) 174–182.

[41] M.J. Rice, A.K. Chakraborty, A.T. Bell, J. Catal. 186 (1999) 222–227.

[42] B. Wichterlova, J. Dědeček, Z. Sobalík, A. Vondrova, K. Klier, J. Catal. 169 (1997) 194–202.

[43] H.-Y. Chen, Z. Wei, M. Kollar, F. Gao, Y. Wang, J. Szanyi, C.H. Peden, Catal. Today 267 (2016) 17–27.

[44] B. Pommier, P. Gelin, Phys. Chem. Chem. Phys. 3 (2001) 1138–1143.

[45] B. Pommier, P. Gélin, Phys. Chem. Chem. Phys. 1 (1999) 1665–1672.

[46] B. Stasinska, A. Machocki, K. Antoniak, M. Rotko, J.L. Figueiredo, F. Gonçalves, Catal. Today 137 (2008) 329–334.

[47] R. Burch, F. Urbano, P. Loader, Appl. Catal. A Gen. 123 (1995) 173–184.

[48] Y. Zheng, L. Kovarik, M.H. Engelhard, Y. Wang, Y. Wang, F. Gao, J. Szanyi, J. Phys. Chem. C 121 (2017) 15793–15803.

[49] L. Sheu, H. Knözinger, W. Sachtler, Catal. Lett. 2 (1989) 129–137.

[50] W.M. Sachtler, F.A. Cavalcanti, Z. Zhang, Catal. Lett. 9 (1991) 261–271.

[51] N.K. Nag, J. Phys. Chem. B 105 (2001) 5945–5949.

[52] M. Bonarowska, J. Pielaszek, W. Juszczyk, Z. Karpiński, J. Catal. 195 (2000) 304–315.